Letter

Predicting magnetic edge behavior in graphene using neural networks

Meric E. Kucukbas [1], Seán McCann,[1] and Stephen R. Power [1,2,*]
[1]*School of Physics, Trinity College Dublin, Dublin 2, Ireland*
[2]*School of Physical Sciences, Dublin City University, Glasnevin, Dublin 9, Ireland*

Magnetic moments near zigzag edges in graphene allow complex nanostructures with customized spin properties to be realized. However, computational costs restrict theoretical investigations to small or perfectly periodic structures. Here, we demonstrate that a machine-learning approach, using only geometric input, can accurately estimate magnetic moment profiles, allowing arbitrarily large and disordered systems to be quickly simulated. Excellent agreement is found with mean-field Hubbard calculations, and important electronic, magnetic, and transport properties are reproduced using the estimated profiles. This approach allows the magnetic moments of experimental-scale systems to be quickly and accurately predicted, and will speed up the identification of promising geometries for spintronic applications. While machine-learning approaches to many-body interactions have largely been limited to exact solutions of complex models at very small scales, this Letter establishes that they can be successfully applied at very large scales at mean-field levels of accuracy.

Graphene systems with zigzag (ZZ) edge segments can exhibit magnetic polarization at half filling [1–4]. A ZZ edge hosts a localized state at the Fermi energy [5], which is spin split by electron-electron interactions [2,6]. The resultant magnetic moments decay away from the edge and display an antiferromagnetic (AFM) texture with respect to the sublattice, with different sublattice edges displaying opposite polarizations [1,2,7–9]. Local moment formation and long spin-diffusion lengths together suggest graphene as a promising spintronic material [10], and many device proposals are predicated on ZZ-edge magnetism [2,11–17]. Zigzag graphene nanoribbons (ZGNRs) host spin-polarized transport channels near their edges, which can be further harnessed using electric fields [2] or geometry effects [11,18,19] to induce half-metallic behavior and spin-filtering functionalities. Finite dot structures allow a greater number of edges and more complex behavior [13,20–23]. For example, flakes with a sublattice imbalance can have a net magnetization [7]. Similar behavior is predicted for subtractive antidot systems [24–26], where ZZ-edged perforations underpin half-metallic [27] and anisotropic transport [28].

Magnetic moments decay away from, and vary along, ZZ edges. Maxima are found at the center of extended ZZ sections, with smaller values towards the bulk and near junctions or corners [4,20,21]. While fabrication methods can create edges with preferential orientations [29–35], most experimental systems contain a mix of different edge lengths and types [36–39]. The coupling between states at these edges can lead to complex magnetic profiles, as demonstrated in Fig. 1. Until recently [40], direct experimental evidence of local magnetism had proven elusive, and most studies rely on indirect scanning tunneling signatures [33,35,41]. These

depend sensitively on the system geometry, and measurements are usually compared to theoretical calculations to verify the presence of magnetism. Moment profiles can be simulated using spin-polarized density functional theory (DFT) if the system is periodic or very small. Larger systems can be considered using a tight-binding (TB) approach with a mean-field Hubbard term. However, this scales poorly due to repeated diagonalization of large matrices in the self-consistent (SC) procedure, curtailing efforts to investigate large or disordered systems.

In this Letter, we propose a machine-learning (ML) approach to estimate moment profiles entirely from geometric considerations. We develop a simple descriptor which captures the location of a site relative to nearby edges of various types, and which also encodes the important sublattice texture of such systems (Fig. 1). We demonstrate that neural networks can quickly and accurately estimate local moments using this descriptor, removing a significant computational bottleneck to investigating magnetic graphene systems. Our method reliably reproduces a range of electronic and magnetic quantities, and is easily transferable to other spatially varying properties. Finally, we apply our method to an important open question: Will spin transport near edges survive in realistic systems? We find that this crucial behavior is surprisingly robust against long-ranged width fluctuations, which have been observed experimentally [34].

Method. A library of 4505 graphene flakes was created, containing both regular (finite ZGNRs) and irregular (many-sided polygons and edge-disordered dots) geometries. This contains a variety of flake sizes (50–9000 atoms), edge lengths, and edge types. The system in Fig. 1 is produced by the polygon method, with other examples given in the Supplemental Material (SM) [42]. Each site in a flake is classified as either "bulk" or one of three edge types: "zigzag," "corner," or "armchair" [43]. A nearest-neighbor TB model describes

*stephen.r.power@dcu.ie
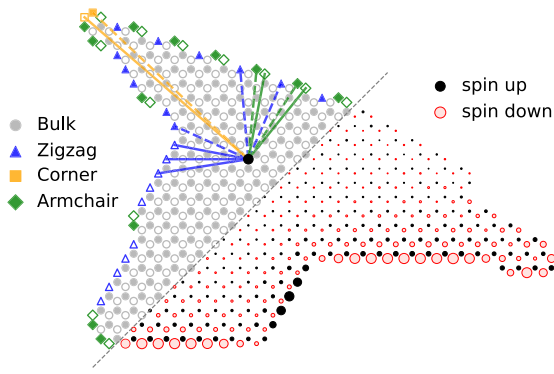
FIG. 1. Left: Site types within a disordered graphene flake, with sublattices shown by solid or open symbols. Lines show the nearest edge sites (of each type) to the black circle. Right: Self-consistently calculated moments in the flake, with size (color) denoting the moment magnitude (sign).

FIG. 2. (a) Comparison of actual and NN-predicted moment magnitudes for every site, in every flake, in the test set. (b), (c) Mean absolute error of the test set for different numbers of sites in full and partial-type descriptors. (d), (e) Maps of the actual moments and the deviation of the predicted moments for a test system. (f) Comparison of spin-polarized energy levels of this system calculated using the actual (solid lines) or predicted moment profiles (dashed lines), with the nonmagnetic (NM) levels (gray lines).

the electronic structure of the flakes, with an on-site Hubbard term capturing electron-electron interactions. Within the mean-field approximation, this reduces to a spin-dependent on-site potential $\epsilon_{i\sigma} = -\sigma\frac{U}{2}m_i$ at each site i, where m_i is the local moment and a Hubbard parameter $U = 1.33|t|$ gives results in good agreement with DFT calculations [3]. In this Letter, we consider the energetically favorable AFM solution and restrict our focus to the undoped case with half-filled p_z orbitals. The values of m_i are calculated by a self-consistent (SC) procedure [42], starting from an initial trial solution.

The SC calculation creates a mapping from a flake geometry, via the Hamiltonian, to a moment profile. Deep neural networks can be a powerful tool to approximate such mappings where they are unknown or prohibitively expensive to calculate. Layers of artificial neurons are exposed to a training data, and have their parameters adjusted to minimize the error between the output and the expected result. A network is tested on unseen data during ("validation") and after ("test") the training process to prevent overfitting and establish its accuracy. Such methods have been used to estimate *ab initio* figures of merit for materials design [44,45], reproduce functionals in complex many-body models [46], and predict critical behavior in lattices [47,48]. In graphene systems, ML approaches have been employed to predict the effects of disorder [49], strain [50,51], or doping [52].

Since magnetic moments are largely influenced by local geometric details, we train neural networks [53,54] to return individual site moments, based on local descriptors, rather than the moment profiles of entire structures. This allows trained models to be easily applied to systems of arbitrary size. Our "partial" descriptor for a site contains the distances to the (N_Z, N_C, N_A) nearest edge sites of zigzag, corner, and armchair type, respectively, for both the same and opposite sublattices as the relevant site. A "full" descriptor also contains the distances between these edge sites. In each case, the shortest path between two sites in the lattice is used as the distance metric, which captures the connectivity of the lattice and is important for complex geometries. The descriptors are invariant under rotations and translations. The network is trained to identify the absolute value of a moment, with its

sign determined by sublattice. See SM [42] for more details on descriptor generation, and for code to make moment predictions for arbitrary geometries.

The actual moments for all 271 590 sites in the 451 test set flakes are compared to those predicted by the most accurate of the trained neural networks in Fig. 2(a), which uses a full descriptor with $N_Z = 11$, $N_A = 3$, $N_C = 5$. The distribution is maximal along the diagonal and decays rapidly away from it, showing an excellent correspondence between predicted and actual moments. We now consider how the accuracy achieved depends on the descriptor details. Unsurprisingly, the mean absolute error (MAE) decreases as N_Z increases, adding more ZZ site information to the descriptor, while keeping N_C and N_A fixed [Fig. 2(b)]. Although they are not typically associated with edge magnetism, Fig. 2(c) shows that information about other edge types is also essential. Armchair and corner sites can occur at the end of ZZ segments, and help indicate the length of a ZZ edge. Full descriptors, by including all the pairwise edge site separations, give a much more complete description of the edge structure near a site. They give a significant improvement over partial descriptors, containing only the distances to the site of interest, but typically require larger networks and more memory and training time. While the MAE is a useful metric to compare networks trained on the same sets, as above, its magnitude largely depends on the specific flakes in the test set. Perhaps more insightful is the MAE on all edge sites in irregular flakes, which for our optimal network is $\sim 7 \times 10^{-3}\mu_B$, or less than 3% of the edge moment in a pristine ZGNR [42].

Generalization. The actual moments in a polygon flake from the test set and the prediction error at each site are
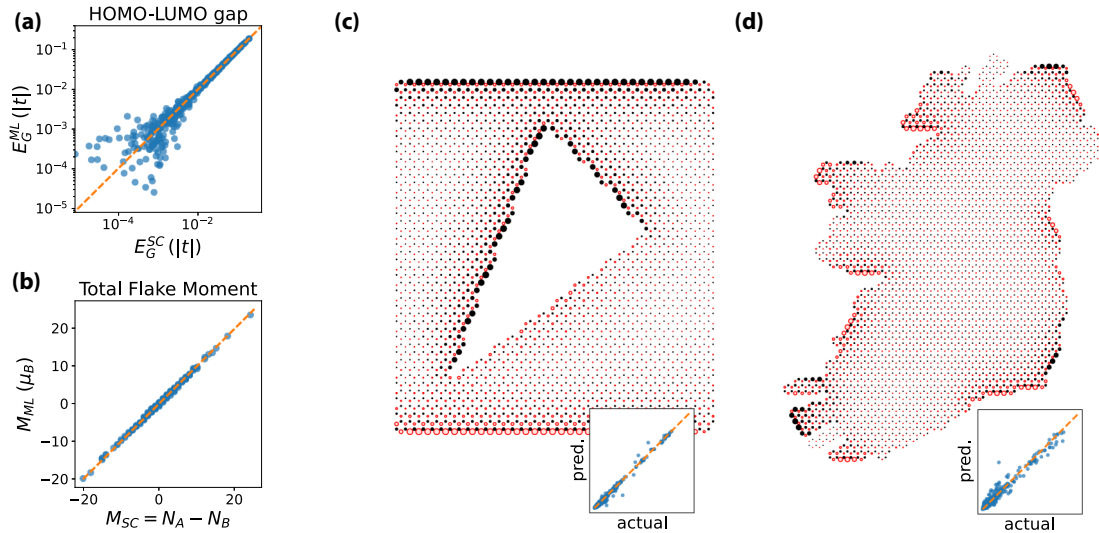
FIG. 3. (a), (b) Comparison of the spin-split band gap and the total magnetic moment of each flake in the test set, calculated using moments from both self-consistent (SC) and machine-learning (ML) methods. (c), (d) Predicted moments for geometries with features, such as internal edges and rugged peninsulas, which are not present in the training set. The insets compare the actual and predicted moments in each system.

mapped in Figs. 2(d) and 2(e). The predicted moments follow the expected trends, i.e., decay from the center of long zigzag edges towards the bulk or other edge types, and have an excellent quantitative match with the actual moments with discrepancies at only very few sites. Since the network is only given local site information, it is not aware of the overall size, shape, or edge lengths of a flake. However, many quantities depend on the moment profile of the entire flake, and if sufficiently accurate, more-or-less instantaneous ML predictions would allow us to circumvent the SC computational bottlenecks. Energy spectra of the considered flake are shown in Fig. 2(f), with the dashed black and red lines showing the up- and down-spin levels calculated using ML moments. They align almost perfectly with results using exact SC moment profiles (solid lines). Comparison with the nonmagnetic case (gray lines) shows that the ML levels accurately capture both the qualitative and quantitative features of the spectrum, including the spin splitting of zero-energy states and the overall level distribution.

The band gap E_G of a flake can be enhanced by spin splitting, and is sometimes taken as a proxy for local magnetism in experiments [33]. Figure 3(a) compares E_G (in log scale), calculated using both SC and ML moment profiles, for every test set flake. The ML moments give a highly accuracy estimate once $E_G \gtrsim 0.01|t| \sim 30$ meV, with an average error of $\sim 3\%$. The total magnetic moment M of a flake is also of interest, since the SC value exactly obeys Lieb's theorem [7] and is given by the difference between the number of A and B sublattice sites: $M = N_A - N_B$. Site-by-site ML estimates place no constraints on M, nonetheless Fig. 3(b) shows excellent agreement with SC results and Lieb's theorem.

The ML approach clearly allows for quick and reliable estimations of systemwide properties relevant to both theoretical and experimental studies. The model successfully generalizes to flakes similar to those on which it was trained, but as these do not include every possible kind of edge profile, it is worth examining its performance outside the test set. Figure 3(c)

contains an internal perforation, none of which are present in the training set, and which increases the complexity of the moment profile. Nonetheless the network is able to accurately reproduce the SC result. Key to its success is the distance metric used in the descriptor, which prevents undue influence between sites separated by the perforation. This is also important for the geometry in Fig. 3(d), based on the coastline of Ireland. This contains a mix of edges, angles, and local disorders that do not emerge from the simpler etching methods. ML predictions again agree with full calculations, and in particular capture complex behavior where parallel peninsulas give large numbers of nearby edge sites.

Application to spin transport. Finite flakes are a useful platform for building a ML model, but applicability is limited without generalization to extended ribbons, which underpin the majority of proposed devices. Local defects, functionalizations, and reconstructions can inhibit moment formation or backscatter electrons near the edge, removing the desired behavior [11,55–57]. State-of-the-art epitaxial [17,34] and bottom-up grown ribbons [29,32,35], where such strong local disorders are largely absent, nonetheless include longer-ranged disorders, such as smooth width fluctuations or irregular junctions. Edge roughness has been extensively studied in nonmagnetic ribbons and typically requires configurational averaging over large numbers of ZGNRs [58]. This prevents similar studies in magnetic ribbons, as calculating the required moment profiles is prohibitively expensive. This cost can now be allayed using accurate ML moments, enabling the study of spin-polarized transport in experimental-scale disordered ZGNRs.

The device in Fig. 4(a) contains smooth width fluctuations similar to experimental systems [17,39]. It is also near the upper limit of systems that can be solved self-consistently, allowing us to benchmark ML results. The inset confirms the excellent generalization of the ML model to this system, which manifests as an almost perfect agreement between transmission calculations using ML (lines) and SC (dots)
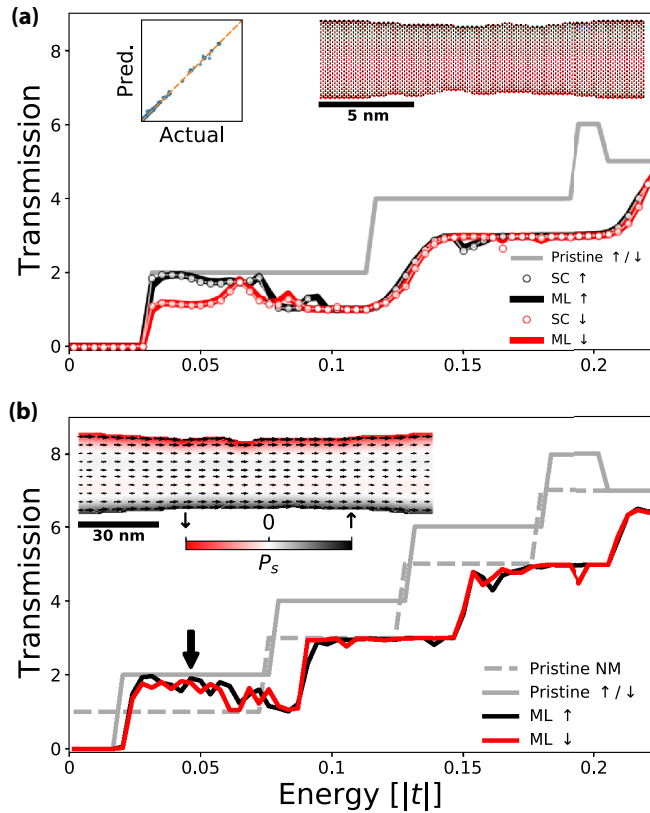
FIG. 4. (a) Spin-dependent transmission in an edge-disordered ZGNR, calculated using SC (symbols) and ML (lines) moment profiles. The insets show the accuracy of the ML moments and the moment profile along the ribbon. (b) Transmissions through a larger system. The inset maps the current flow and spin polarization at the marked energy. Spin-polarized channels are visible along the rough edges.

moments. Machine learning is being used here to predict moment profiles, not to directly estimate transmission [49] as this can be efficiently calculated using recursive techniques [42,59] once the moments are known. Since ML moments are sufficiently accurate for transport calculations, we now scale up to larger systems that would otherwise be computationally intractable. Figure 4(b) investigates such a system using ML-predicted moments only. Without edge disorder, the transmission (per spin) is higher in a magnetic (solid gray) than a nonmagnetic ribbon (dashed gray) in the range $0.02|t| \lesssim E \lesssim 0.2|t|$. This is due to an additional dispersive edge mode, arising from spin splitting of a flat band in the nonmagnetic system.

Comparing the disordered spin-dependent results to both pristine cases allows us to explain the effect of edge roughness. At energies $E \gtrsim 0.1|t|$, the disordered transmissions return to the sequence seen for NM ribbons, suggesting that the spin-polarized edge mode has been completely quenched. The other modes are robust against smooth disorder, so the plateau behavior persists, but with an energy shift caused by mode matching between sections with different widths. Very different behavior is seen at low energies, e.g., at the arrow in Fig. 4(b), where the disordered spin-dependent cases show

near perfect transmission. The persistence of spin transport here is due to a lack of backscattering possibilities. The left- and right-propagating modes for a given spin are located on the same edge, so scattering between these modes can occur without a spin flip. However, these two modes are associated with widely separated states in reciprocal space, so that scattering between them requires short-ranged disorder, which is not present here. The only other mode at this energy has very little edge component, which limits backscattering into it.

This suppression of backscattering allows spin-polarized transport in edge channels to persist, as shown explicitly in the inset map, which plots the local current flow (arrows) and spin polarization (colour) for the marked energy. While spin transport survives at low energies, it vanishes at higher energies due to the onset of higher-order bulk modes which offer additional backscattering possibilities. These results provide a useful insight for experimental device design: The desired spintronic behavior can also appear for rough edges, but in a more limited energy range than for pristine systems.

Conclusions. Neural networks gives a quick and reliable estimate of the mean-field solution to the Hubbard model in a half-filled bipartite lattice. Prediction cost scales linearly with system size, allowing for rapid calculations in systems that were previously intractable. Immediate applications lie in the study of graphene edge magnetism, where the electronic, magnetic, and transport properties of a wide range of systems can be efficiently and accurately calculated. Given the excellent generalization of the model, both to geometries and quantities unseen during training, it can be applied to a number of problems. It allows for a detailed analysis of transport in disordered GNRs, where understanding the interplay between large-scale disorder and local magnetism is essential if GNRs are to play their mooted roles in electronic, spintronic, and quantum devices. To help achieve this, we have made available sample code to quickly apply our model and predict moments for arbitrary geometries [42].

Our approach can also act as a starting point for more accurate studies or more complex problems. ML profiles can be used as almost-converged "initial guesses" in SC calculations, reducing the number of steps required. More accurate ML estimates may also be achieved by supplementing the simple geometric information in our descriptors. For example, moment formation is strongly tied to the local density of states [60], so including a non-SC evaluation of this quantity could improve model performance. A trade-off will emerge here between the extra time needed to generate the descriptor and the accuracy required. These strategies were not needed to achieve high accuracy in this work, but could help in more complicated cases. Examples include lattices away from half filling, with nonuniform background potentials, or of different materials, where exact solutions are difficult to calculate and display less intuitive trends.

Finally, we focused here on material properties at the nano- and mesoscopic scales where graphene systems are investigated experimentally and incorporated into devices. This is in contrast to previous studies using ML to consider more fundamental aspects of the Hubbard model [46,61], which typically consider smaller systems in which exact solutions can be found. However, the techniques developed here are

not scale specific and may also find applicability in advanced many-body models.

[1] M. Fujita, K. Wakabayashi, K. Nakada, and K. Kusakabe, Peculiar localized state at zigzag graphite edge, J. Phys. Soc. Jpn. **65**, 1920 (1996).

[2] Y.-W. Son, M. L. Cohen, and S. G. Louie, Half-metallic graphene nanoribbons, Nature (London) **444**, 347 (2006).

[3] O. V. Yazyev, Emergence of magnetism in graphene materials and nanostructures, Rep. Prog. Phys. **73**, 056501 (2010).

[4] O. V. Yazyev, R. B. Capaz, and S. G. Louie, Theory of magnetic edge states in chiral graphene nanoribbons, Phys. Rev. B **84**, 115406 (2011).

[5] K. Nakada, M. Fujita, G. Dresselhaus, and M. S. Dresselhaus, Edge state in graphene ribbons: Nanometer size effect and edge shape dependence, Phys. Rev. B **54**, 17954 (1996).

[6] Y.-W. Son, M. L. Cohen, and S. G. Louie, Energy Gaps in Graphene Nanoribbons, Phys. Rev. Lett. **97**, 216803 (2006).

[7] E. H. Lieb, Two theorems on the Hubbard model, Phys. Rev. Lett. **62**, 1201 (1989).

[8] J. J. Palacios, J. Fernández-Rossier, and L. Brey, Vacancy-induced magnetism in graphene and graphene ribbons, Phys. Rev. B **77**, 195428 (2008).

[9] D. Yu, E. M. Lupton, H. J. Gao, C. Zhang, and F. Liu, A unified geometric rule for designing nanomagnetism in graphene, Nano Res. **1**, 497 (2008).

[10] W. Han, R. K. Kawakami, M. Gmitra, and J. Fabian, Graphene spintronics, Nat. Nanotechnol. **9**, 794 (2014).

[11] M. Wimmer, I. Adagideli, S. Berber, D. Tománek, and K. Richter, Spin Currents in Rough Graphene Nanoribbons: Universal Fluctuations and Spin Injection, Phys. Rev. Lett. **100**, 177207 (2008).

[12] J. Guo, D. Gunlycke, and C. T. White, Field effect on spin-polarized transport in graphene nanoribbons, Appl. Phys. Lett. **92**, 163109 (2008).

[13] W. L. Wang, O. V. Yazyev, S. Meng, and E. Kaxiras, Topological Frustration in Graphene Nanoflakes: Magnetic Order and Spin Logic Devices, Phys. Rev. Lett. **102**, 157201 (2009).

[14] X. Lü, Y. Zheng, H. Xin, and L. Jiang, Spin polarized electron transport through a graphene nanojunction, Appl. Phys. Lett. **96**, 132108 (2010).

[15] T. Ozaki, K. Nishio, H. Weng, and H. Kino, Dual spin filter effect in a zigzag graphene nanoribbon, Phys. Rev. B **81**, 075422 (2010).

[16] A. Saffarzadeh and R. Farghadan, A spin-filter device based on armchair graphene nanoribbons, Appl. Phys. Lett. **98**, 023106 (2011).

[17] J. Aprojanz, S. R. Power, P. Bampoulis, S. Roche, A.-P. Jauho, H. J. W. Zandvliet, A. A. Zakharov, and C. Tegenkamp, Ballistic tracks in graphene nanoribbons, Nat. Commun. **9**, 4426 (2018).

[18] Q. Sun, X. Yao, O. Gröning, K. Eimre, C. A. Pignedoli, K. Müllen, A. Narita, R. Fasel, and P. Ruffieux, Coupled spin states in armchair graphene nanoribbons with asymmetric zigzag edge extensions, Nano Lett. **20**, 6429 (2020).

[19] J. Jiang and S. G. Louie, Topology classification using chiral symmetry and spin correlations in graphene nanoribbons, Nano Lett. **21**, 197 (2021).

[20] J. Fernández-Rossier and J. J. Palacios, Magnetism in Graphene Nanoislands, Phys. Rev. Lett. **99**, 177204 (2007).

[21] S. Bhowmick and V. B. Shenoy, Edge state magnetism of single layer graphene nanostructures, J. Chem. Phys. **128**, 244717 (2008).

[22] M. Wimmer, A. R. Akhmerov, and F. Guinea, Robustness of edge states in graphene quantum dots, Phys. Rev. B **82**, 045409 (2010).

[23] P. Potasz, A. D. Güçlü, A. Wójs, and P. Hawrylak, Electronic properties of gated triangular graphene quantum dots: Magnetism, correlations, and geometrical effects, Phys. Rev. B **85**, 075431 (2012).

[24] D. Yu, E. M. Lupton, M. Liu, W. Liu, and F. Liu, Collective magnetic behavior of graphene nanohole superlattices, Nano Res. **1**, 56 (2008).

[25] X. H. Zheng, G. R. Zhang, Z. Zeng, V. M. García-Suárez, and C. J. Lambert, Effects of antidots on the transport properties of graphene nanoribbons, Phys. Rev. B **80**, 075413 (2009).

[26] M. L. Trolle, U. S. Møller, and T. G. Pedersen, Large and stable band gaps in spin-polarized graphene antidot lattices, Phys. Rev. B **88**, 195418 (2013).

[27] S. S. Gregersen, S. R. Power, and A.-P. Jauho, Nanostructured graphene for spintronics, Phys. Rev. B **95**, 121406(R) (2017).

[28] S. S. Gregersen, J. H. Garcia, A. P. Jauho, S. Roche, and S. R. Power, Charge and spin transport anisotropy in nanopatterned graphene, J. Phys. Mater. **1**, 015005 (2018).

[29] X. Li, X. Wang, L. Zhang, S. Lee, and H. Dai, Chemically derived, ultrasmooth graphene nanoribbon semiconductors, Science **319**, 1229 (2008).

[30] D. V. Kosynkin, A. L. Higginbotham, A. Sinitskii, J. R. Lomeda, A. Dimiev, B. K. Price, and J. M. Tour, Longitudinal unzipping of carbon nanotubes to form graphene nanoribbons, Nature (London) **458**, 872 (2009).

[31] X. Jia, M. Hofmann, V. Meunier, B. G. Sumpter, J. Campos-Delgado, J. M. Romo-Herrera, H. Son, Y.-P. Hsieh, A. Reina, J. Kong, M. Terrones, and M. S. Dresselhaus, Controlled formation of sharp zigzag and armchair edges in graphitic nanoribbons, Science **323**, 1701 (2009).

[32] J. Cai, P. Ruffieux, R. Jaafar, M. Bieri, T. Braun, S. Blankenburg, M. Muoth, A. P. Seitsonen, M. Saleh, X. Feng, K. Müllen, and R. Fasel, Atomically precise bottom-up fabrication of graphene nanoribbons, Nature (London) **466**, 470 (2010).

[33] G. Z. Magda, X. Jin, I. Hagymási, P. Vancsó, Z. Osváth, P. Nemes-Incze, C. Hwang, L. P. Biró, and L. Tapasztó, Room-temperature magnetic order on zigzag edges of narrow graphene nanoribbons, Nature (London) **514**, 608 (2014).

[34] J. Baringhaus, M. Ruan, F. Edler, A. Tejeda, M. Sicot, A. Taleb-Ibrahimi, A.-P. Li, Z. Jiang, E. H. Conrad, C. Berger, C. Tegenkamp, and W. A. de Heer, Exceptional ballistic transport in epitaxial graphene nanoribbons, Nature (London) **506**, 349 (2014).

[35] P. Ruffieux, S. Wang, B. Yang, C. Sanchez-Sanchez, J. Liu, T. Dienel, L. Talirz, P. Shinde, C. A. Pignedoli, D. Passerone, T. Dumslaff, X. Feng, K. Müllen, and R. Fasel, On-surface synthesis of graphene nanoribbons with zigzag edge topology, Nature (London) **531**, 489 (2016).

[36] M. Y. Han, B. Özyilmaz, Y. Zhang, and P. Kim, Energy Band-Gap Engineering of Graphene Nanoribbons, Phys. Rev. Lett. **98**, 206805 (2007).

[37] N. Tombros, A. Veligura, J. Junesch, M. H. D. Guimarães, I. J. Vera-Marun, H. T. Jonkman, and B. J. van Wees, Quantized conductance of a suspended graphene nanoconstriction, Nat. Phys. **7**, 697 (2011).

[38] B. Terrés, L. A. Chizhova, F. Libisch, J. Peiro, D. Jörger, S. Engels, A. Girschik, K. Watanabe, T. Taniguchi, S. V. Rotkin, J. Burgdörfer, and C. Stampfer, Size quantization of Dirac fermions in graphene constrictions, Nat. Commun. **7**, 11528 (2016).

[39] J. M. Caridad, S. R. Power, M. R. Lotz, A. A. Shylau, J. D. Thomsen, L. Gammelgaard, T. J. Booth, A.-P. Jauho, and P. Bøggild, Conductance quantization suppression in the quantum Hall regime, Nat. Commun. **9**, 659 (2018).

[40] S. Mishra, D. Beyer, K. Eimre, S. Kezilebieke, R. Berger, O. Gröning, C. A. Pignedoli, K. Müllen, P. Liljeroth, P. Ruffieux, X. Feng, and R. Fasel, Topological frustration induces unconventional magnetism in a nanographene, Nat. Nanotechnol. **15**, 22 (2020).

[41] C. Tao, L. Jiao, O. V. Yazyev, Y. C. Chen, J. Feng, X. Zhang, R. B. Capaz, J. M. Tour, A. Zettl, S. G. Louie, H. Dai, and M. F. Crommie, Spatially resolving edge states of chiral graphene nanoribbons, Nat. Phys. **7**, 616 (2011).

[42] See Supplemental Material at http://link.aps.org/supplemental/10.1103/PhysRevB.106.L081411 for more method details and additional results.

[43] A. K. Singh, E. S. Penev, and B. I. Yakobson, Armchair or zigzag? A tool for characterizing graphene edge, Comput. Phys. Commun. **182**, 804 (2011).

[44] K. Hansen, G. Montavon, F. Biegler, S. Fazli, M. Rupp, M. Scheffler, O. A. von Lilienfeld, A. Tkatchenko, and K.-R. Müller, Assessment and validation of machine learning methods for predicting molecular atomization energies, J. Chem. Theory Comput. **9**, 3404 (2013).

[45] J. Schmidt, M. R. Marques, S. Botti, and M. A. Marques, Recent advances and applications of machine learning in solid-state materials science, npj Comput. Mater. **5**, 83 (2019).

[46] J. Nelson, R. Tiwari, and S. Sanvito, Machine learning density functional theory for the Hubbard model, Phys. Rev. B **99**, 075132 (2019).

[47] J. Carrasquilla and R. G. Melko, Machine learning phases of matter, Nat. Phys. **13**, 431 (2017).

[48] D.-L. Deng, X. Li, and S. Das Sarma, Machine learning topological states, Phys. Rev. B **96**, 195145 (2017).

[49] A. Lopez-Bezanilla and O. A. von Lilienfeld, Modeling electronic quantum transport with machine learning, Phys. Rev. B **89**, 235411 (2014).

[50] V. Torres, P. Silva, E. A. T. de Souza, L. A. Silva, and D. A. Bahamon, Valley notch filter in a graphene strain superlattice: Green's function and machine learning approach, Phys. Rev. B **100**, 205411 (2019).

[51] J. G. Nedell, J. Spector, A. Abbout, M. Vogl, and G. A. Fiete, Deep learning of deformation-dependent conductance in thin films: Nanobubbles in graphene, Phys. Rev. B **105**, 075425 (2022).

[52] K. Ryczko, P. Darancet, and I. Tamblyn, Inverse design of a graphene-based quantum transducer via neuroevolution, J. Phys. Chem. C **124**, 26117 (2020).

[53] M. Abadi, A. Agarwal, P. Barham, E. Brevdo, Z. Chen, C. Citro, G. S. Corrado, A. Davis, J. Dean, M. Devin, S. Ghemawat, I. Goodfellow, A. Harp, G. Irving, M. Isard, Y. Jia, R. Jozefowicz, L. Kaiser, M. Kudlur, J. Levenberg *et al.*, TensorFlow: Large-scale machine learning on heterogeneous systems (2015), software available from tensorflow.org.

[54] F. Chollet *et al.*, Keras, https://keras.io.

[55] B. Huang, F. Liu, J. Wu, B.-L. Gu, and W. Duan, Suppression of spin polarization in graphene nanoribbons by edge defects and impurities, Phys. Rev. B **77**, 153411 (2008).

[56] J. Kunstmann, C. Özdoğan, A. Quandt, and H. Fehske, Stability of edge states and edge magnetism in graphene nanoribbons, Phys. Rev. B **83**, 045414 (2011).

[57] M. Pizzochero, G. B. Barin, K. Čerņevičs, S. Wang, P. Ruffieux, R. Fasel, and O. V. Yazyev, Edge disorder in bottom-up zigzag graphene nanoribbons: Implications for magnetism and quantum electronic transport, J. Phys. Chem. Lett. **12**, 4692 (2021).

[58] E. R. Mucciolo, A. H. Castro Neto, and C. H. Lewenkopf, Conductance quantization and transport gaps in disordered graphene nanoribbons, Phys. Rev. B **79**, 075407 (2009).

[59] N. Papior, N. Lorente, T. Frederiksen, A. García, and M. Brandbyge, Improvements on non-equilibrium and transport Green function techniques: The next-generation transiesta, Comput. Phys. Commun. **212**, 8 (2017).

[60] P. W. Anderson, Localized magnetic states in metals, Phys. Rev. **124**, 41 (1961).

[61] H. Saito, Solving the Bose-Hubbard model with machine learning, J. Phys. Soc. Jpn. **86**, 093001 (2017).